University of Wah Journal of Science and Technology Vol. 8 (2024), PP 52-65.
ISSN: 2523-0123 (Print) 2616-4396 (Online)

University of Wah
Journal of Science and Technology

www.uow.edu.pk

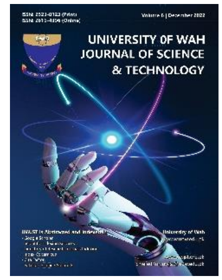

Influence of magnetic oxide nanoparticles in Couette flow through silver metallic plates with constant suction

Zaheer Abbas[1], Muhammad Farhan[1], Muhammad Yousaf Rafiq*[1] and Muhammad Shakib Arslan[1]
[1] Department of Mathematics, Faculty of Physical and Mathematical Science, The Islamia University of Bahawalpur, Pakistan.
*Corresponding author e-mail: jamyousaf631@gmail.com

Abstract
This article explores the influence of magnetohydrodynamics on the Couette flow of viscous nanofluid having magnetic oxide nanoparticles suspension through parallel metallic silver plates with constant suction at the lower plate. The modeled equations of viscous nanofluid of Couette flow are simplified in their dimensionless form using similarity transformations. The exact solutions for the pressure gradient, radial velocity, and axial velocity are attained by the separation of variables method. The graphical behavior of embedded parameters on axial and radial velocity is illustrated and discussed in detail. It is seen that axial velocity reduces with an enhancement in the rotation parameter. The implications of this study encompass innovative thermal duct processing technologies within fields such as biomedical, nuclear, and process engineering.

Keywords
Couette flow, angular rotation, nanofluid, inclined magnetic field, silver metallic plates.

NOMENCLATURE			
o	center of plates	ρ	density of fluid
v	kinematic viscosity	σ	electrical conductivity
p	pressure	μ	dynamic viscosity
B_0	strength of the magnetic field	t	time in the fixed frame
u,v	axial and radial components of velocity		Dimensionless Symbols
K	permeability of porous medium	α	viscosity parameter
ψ	stream function	M	magnetic parameter
ω	frequency	S	Darcy parameter
Ω	angular velocity	K_r	rotation parameter
$U(0)$	the average velocity of the fluid	Re	Reynolds number
x, y	Cartesian coordinates	ϕ	nanoparticles volume fraction

1. Introduction

A nanofluid is a colloidal combination comprising nano-sized particles suspended in a base liquid. These nanoparticles are commonly composed of materials like carbon nanotubes, metal oxides, metals, and oxides, while familiar base liquids include water-based H_2O fuels and glycols. The main objective in creating nanofluids is to augment the heat conduction of the liquid. This augmented thermal behavior of nanoparticles has led to a wide range of biomedical and industrial applications. Examples include drag reduction, engine cooling, refrigerants in household fridges, cooling systems for machinery like diesel generators and engine transmissions, and even jacketed water coolers. By utilizing nanofluids with improved heat transfer characteristics, it becomes possible to design engines that function efficiently at optimal temperatures, allowing for the use of smaller and lighter radiators, drives, and other vehicle components. Enhancing heat transfer coefficients through nanofluids can result in lighter automobiles with better fuel economy due to reduced pumping power requirements. Even a modest one percent enhancement in the cooling efficiency of a bus's cooling system could save up to five million barrels of oil annually in the US. Moreover, nanofluids have garnered significant attention for their potential in deep drilling applications. Leveraging the superior thermal conductivity of nanofluids, these liquids find practical use in fields such as electronics, automotive technology, and solar energy. Notably, nanofluids also hold considerable promise in the medical domain. They are employed for drug delivery and the destruction of tumor cells. [1] pioneered the experimental description of liquid thermal conductivity in the presence of nanoparticles. The utilization of the both perturbation scheme and the homotopy technique to analyze transfer heat within a nanofluid movement confined between parallel plates was considered by [2]. [3] analyzed the flow of nanoparticles with base liquid in a vertical plate with heating phenomena. [4] inspected the combined impacts of magnetohydrodynamics on a non-Newtonian nanofluid confined between two rotating plates. [5] scrutinized the heat and mass transfer phenomenon of metallic–liquid nanoparticles between parallel plates influenced by an applied magnetic field as well as a chemical reaction. The influence of aurum and argentum nanoparticles in viscous and mass transfer movements with varying surface forces was inspected by [6]. Various researchers have contributed to the development of distinct facets within these nanofluid models can be seen [7-10].

Magnetohydrodynamics (MHD) can be conceptualized as a vector field that governs the magnetic impact on dynamic rechargeable processes, electric currents, and magnetic characteristics. In MHD, an influencing force acts perpendicular to both the MHD field and the velocity of the force. [11] studied the joint influences of magnetohydrodynamics and radiation on the free convection flow adjacent to a suddenly initiated isothermal vertical plate using the Rosseland diffusion approximation. The motion of a second-grade fluid under magnetohydrodynamic (MHD) conditions on an inclined heated plate with oriented magnetohydrodynamics was reviewed by [12]. [13] studied the magnetohydrodynamic convection-less transport of a Jeffrey fluid over an infinitely extended perpendicular plate, considering both mass and heat transfer. The influence of thermal radiation on the boundary layer flow of a non-Newtonian liquid in the presence of electromagnetic field and Joule heating was observed by [14]. Transient transport of electrically conducting fluid over a flat plate was scrutinized by [15]. [16] investigated the impacts of magnetohydrodynamic forces on the laminar movement of a multi-dimensional nanofluid influenced by radiation in a porous material. [17] examined the three-dimensional magnetohydrodynamic flow of a nanofluid with a couple of stress, considering the influence of thermophoresis and Brownian motion effects. The simulation of magnetohydrodynamic nanoliquid movement within a porous cavity with a heated elliptical obstacle was inspected [18]. [19] explored the natural convection magnetohydrodynamic movement of Casson liquid adjacent to an oscillating vertical plate in a rotating system. [20] inspected entropy generation in the context of magnetohydrodynamic flow of viscous fluid within a vertical porous channel with thermal radiation. [21] scrutinized the unsteady magnetohydrodynamic Couette movement between silver metallic parallel plates. The system involves constant periodic suction applied to the lowermost permeable metallic shield, influenced by a magnetic field with inclination and system rotation. A numerical analysis is performed on the magnetohydrodynamic nanoliquid movement and heated within a rounded permeable medium featuring a Cassini oval. The study considers the impact of both Lorentz and buoyancy forces was discussed by [22]. [23] investigated the magnetized movement of heated non-Newtonian liquid over a perpendicular geometry. [24] explored the influence of a hybrid nanofluid considering factors such as magnetohydrodynamics, and heated, as it flows past a porous tinny needle. The influence of slip motion of an electrically conducting MHD non-Newtonian liquid within a conduit was elaborated [25]. [26] analyzed unsteady magnetohydrodynamic liquid movement between two parallel discs with constant oscillation, considering stimulation energy and modified Hall impact. Entropy generation in the unsteady magnetohydrodynamic nanoliquid movement past a revolving porous plate was studied by [27].

To the best of the author's acquaintance, there is no existing study in the literature that explores unsteady Couette flow of nanofluid through silver metallic parallel plates with constant suction at the lower plate. Consequently, conducting a comparative study in this specific context is challenging. With this motivation, this inquiry aims to emphasize the significance of the time-dependent incompressible Couette movement of viscous nanoparticles through silver metallic parallel plates with constant suction at the lower plate. The problem was addressed by employing similarity transformation, leading to the derivation of an analytical solution for the relevant boundary conditions. The axial and radial velocity profiles are provided and examined. Finally, graphical representations illustrate the variations in different relevant parameters. The novelty of the present problem is its unique approach of simultaneously accounting for magnetohydrodynamics, nanofluid rheology, and the presence of magnetic oxide nanoparticles combination that has not been explored in the existing literature. The main objective of this research is summarized as:

- The investigation assesses the inclusion of nanoparticles in the ferric oxide base liquid as the volume fraction increases.
- The influence of the magnetohydrodynamic parameter on flow characteristics is examined.
- The effects of suction on the couette flow of nanoliquid are analyzed.
- The flow behavior is examined in the presence of silver metallic parallel plates.
- The study explores whether an angular rotation exhibits similar solutions.
- The suction parameter enhances the axial velocity.

2. Geometric model

As depicted in Fig. 1, when considering the synchronized system in Cartesian coordinates, we assume that a time-dependent magnetized nanoliquid is moving along the x-axis parallel to silver metallic plates. The two silver metallic plates are separated by a distance denoted as $2h,$ where the lower stationary permeable silver metallic plate is situated at $y=-h,$ and the upper silver metallic plate is consistently in motion at $y=h.$ The application scenario involves the controlled flow of a viscous liquid with an initial average velocity between the silver metallic parallel plates. Simultaneously, a transverse magnetic field is applied perpendicular to both the silver metallic plates and the direction of the fluid flow. This configuration can find practical applications in various fields such as magneto hydrodynamics, fluid dynamics, or heat transfer, where the interaction between magnetic fields and fluid flow is of interest. Potential applications could include the development of efficient heat exchangers, fluid-based sensors, or devices that utilize magnetic fields to manipulate and control the behavior of the flowing liquid within confined spaces. This magnetic field influences the flow field at various inclination angles θ in the presence of constant suction at the lower porous silver metallic plate. The equations that govern the flow of viscous fluid can be formulated as follows:

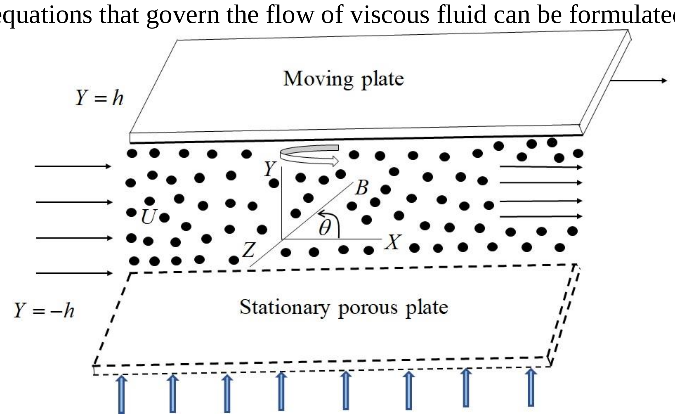

Fig. 1: *Couette flow Geometry*

The equations of the governing problem are expressed as [19]:

$$\frac{\partial u}{\partial x}+\frac{\partial u}{\partial y}=0, \tag{1}$$

$$\frac{\partial u}{\partial t}+\frac{1}{\rho_{nf}}\frac{\partial p}{\partial x}=\nu_{nf}\left(\frac{\partial^2 u}{\partial x^2}+\frac{\partial^2 u}{\partial y^2}\right)+\sigma_{nf}B^2Sin^2\left(\theta\right)-\frac{\nu_{nf}u}{K}+2\Omega u, \tag{2}$$

$$\frac{\partial v}{\partial t}+\frac{1}{\rho_{nf}}\frac{\partial p}{\partial y}=\nu_{nf}\left(\frac{\partial^2 v}{\partial x^2}+\frac{\partial^2 v}{\partial y^2}\right), \tag{3}$$

where u and v are the nanofluid flow in x and y directions respectively. ρ_{nf} signifies the density of the nanoparticle, σ_{nf} indicates the electrical conductivity of the nanoparticle, v_{nf} is the kinematic viscosity, ω is the frequency, t is time, and K is the permeability of the porous medium. The boundary conditions at both the upper metallic silver plate and the lower porous metallic silver plates are as follows:

$$\begin{aligned} u(x,h)&=U(0), \qquad u(x,-h)=0,\\ v(x,h)&=0, \qquad v(x,-h)=-v_0. \end{aligned} \tag{4}$$

The similarity variables are defined as

$$\eta=\frac{y}{h},\quad u=e^{i\omega t}u(x,y),\quad v=e^{i\omega t}v(x,y),\qquad p=e^{i\omega t}p(x,y). \tag{5}$$

The thermophysical characteristics of nanofluid are given as [6]:

$$\left(\alpha_{nf}=k_{nf}\frac{1}{(\rho C_p)_{nf}}\right)\sigma_f,\ \rho_{nf}=(1-\phi)\rho_f+\phi\rho_s,\ \beta_{nf}=(1-\phi)\beta_f+\beta_s\phi,\ \mu_{nf}=\mu_f\frac{1}{(1-\phi)^{2.5}},$$

$$(\rho C_p)_{nf}=(\rho C_p)_s(1-\phi),\ \frac{\sigma_{nf}}{\sigma_f}=1+\frac{3\left(\frac{\sigma_s}{\sigma_f}-1\right)\phi}{\left(\frac{\sigma_s}{\sigma_f}+2\right)-\left(\frac{\sigma_s}{\sigma_f}-1\right)\phi},\ \frac{k_{nf}}{k_f}=\frac{k_s+2k_f-2\phi(k_f-k_s)}{k_s+2k_f+2\phi(k_f-k_s)}. \tag{6}$$

where, μ_{nf} is the dynamic viscosity, α_{nf} thermal diffusivity, k_{nf} thermal conductivity, ρ_{nf} density of nanoparticles, $(C_p)_{nf}$ the specific heat capacity of nanofluid, β_{nf} thermal relaxation coefficient of the nanofluid, ϕ is the nanoparticle volume fraction, σ_{nf} Stephen Boltzmann constant of nanofluid s shows the nanosolid particle and f shows the base fluid.

Table 1: The thermos-physical characteristics of water, iron oxide, and Alumina.

Nanoparticles and base fluid	$\rho(\mathrm{kg/m^3})$	$C_p(\mathrm{J/kg\,K})$	$k(\mathrm{W/mk})$	$\beta\times10^{-5}(\mathrm{k^{-1}})$
H_2O	997.1	4179	0.613	21
Fe_3O_4	5180	670	9.7	0.5
Al_2O_3	3970	765	40	0.85

In terms of non-dimensional variables and physical quantities described in Eq. (5), Eqs. (1)-(3) takes theform:

$$\frac{\partial u}{\partial x}+\frac{1}{\eta\rho_{nf}}\frac{\partial v}{\partial\eta}=0, \tag{7}$$

$$i\omega u=-\frac{1}{\rho_{nf}}\frac{\partial p}{\partial x}+\nu_{nf}\left(\frac{\partial^2 u}{\partial x^2}+\frac{1}{h^2}\frac{\partial^2 u}{\partial\eta^2}\right)-\sigma_{nf}\frac{B^2\operatorname{Sin}^2\theta}{\rho_{nf}}u-\frac{\nu_{nf}}{K}u+2\Omega u, \tag{8}$$

$$i\omega v=-\frac{1}{\rho_{nf}h}\frac{\partial p}{\partial\eta}+\frac{\mu_{nf}}{\rho_{nf}}\left(\frac{\partial^2 v}{\partial x^2}+\frac{1}{h^2}\frac{\partial^2 v}{\partial\eta^2}\right). \tag{9}$$

The modified surface conditions can be described as:

$$u(x,\eta=1)=U(0),\qquad v(x,\eta=1)=0,$$
$$u(x,\eta=-1)=0,\qquad v(x,\eta=-1)=-v_0. \tag{10}$$

Stream function (ψ) is expressed as follows

$$\psi(x,\eta)=(hU-xv_0)\,f(\eta). \tag{11}$$

To satisfy Eq. (5), the axial velocity u and radial velocity v are defined as

$$u(x,y)=\frac{1}{h}\frac{\partial\psi}{\partial\eta}\ \ and\ \ v(x,y)=-\frac{\partial\psi}{\partial x}. \tag{12}$$

By utilizing Eqs. (11-12) transforms into:

$$u=\frac{1}{h}\left(U(0)-\frac{xv_0}{h}\right)f'(\eta)\ \ and\ \ v=f(\eta)v_0. \tag{13}$$

By incorporating the expression from Eq. (13), the Eqs. (5) to (7) are transformed into the subsequent set of differential equations.

$$-\frac{1}{\rho_f A_1}\frac{\partial p}{\partial x}=\left(\left(U-\frac{xv_0}{h}\right)\left(\left(i\omega+\frac{\mu_f}{\rho_f}\frac{1}{k}\frac{A_2}{A_1}-2\Omega\frac{A_3}{A_1}\frac{\sigma_f B^2 Sin^2\theta}{\rho_f}\right)f'(\eta)-\left(\frac{1}{h^2}\frac{\mu_f}{\rho_f}\frac{A_2}{A_1}\right)f'''(\eta)\right)\right), \tag{14}$$

$$-\frac{1}{\rho_f A_1}\frac{\partial p}{\partial\eta}=(i\omega v_0)\,f'(\eta)-\frac{1}{h^2}\frac{\mu_f}{\rho_f}\frac{A_2}{A_1}v_0 f''(\eta). \tag{15}$$

Differentiating Eqs. $(14-15)$ with respect to the variables (η) and (x) respectively yields:

$$\frac{\partial}{\partial\eta}\left(\left(U-\frac{xv_0}{h}\right)\left(\left(i\omega+\frac{\mu_f}{\rho_f}\frac{1}{k}\frac{A_2}{A_1}-2\Omega\frac{A_3}{A_1}\frac{\sigma_f B^2 Sin^2\theta}{\rho_f}\right)f'(\eta)-\left(\frac{1}{h^2}\frac{\mu_f}{\rho_f}\frac{A_2}{A_1}\right)f'''(\eta)\right)\right)+$$
$$\frac{\partial}{\partial\eta}\left(\frac{1}{\rho_f A_1}\frac{\partial p}{\partial x}\right)=0, \tag{16}$$

$$\frac{1}{\rho_f A_1}\frac{\partial^2 p}{\partial x\partial\eta}=0. \tag{17}$$

After integrating Eqs. $(16-17)$ with respect to (η), the resulting equation becomes

$$\left\{\left(i\omega+\frac{\mu_f}{\rho_f}\frac{1}{k}\frac{A_2}{A_1}-2\Omega+\frac{A_3}{A_1}\frac{\sigma_f B^2\,\mathrm{Sin}^2\,\theta}{\rho_f}\right)f'(\eta)-\left(\frac{1}{h^2}\frac{\mu_f}{\rho_f}\frac{A_2}{A_1}\right)f'''(\eta)\right\}=K \tag{18}$$

where, K is an integrating constant. Re-writing the Eq. (18) we obtain

$$f'''(\eta)+\frac{A_1}{A_2}\left(-\frac{iwh^2\rho_f}{\mu_f}+2\Omega\frac{h^2\rho_f}{\mu_f}-\frac{A_2}{A_1}\frac{h^2}{k}+\frac{A_3}{A_1}\frac{\sigma_f}{\rho_f}\frac{B^2Sin^2\theta h^2\rho_f}{\mu_f}\right)f'(\eta)=K, \tag{19}$$

and Eq. (19) written as

$$f'''(\eta)+\left(2K_r\frac{A_1}{A_2}-\alpha^2 h\frac{A_1}{A_2}-M^2\frac{A_3}{A_2}(sin^2(\theta))-\frac{1}{Da}\right)f'(\eta)=K, \tag{20}$$

The conditions at the boundaries (10) transform to

$$f(1)=0,\qquad f'(1)=0,\ \text{and}\ \ f(-1)=-1,\qquad f'(-1)=0. \tag{21}$$

where, $K_r=-i\omega h^2\rho_f/\mu_f$ is the rotation parameter, $M^2=\sigma_f B^2h^2/\mu_f$ is the magnetic parameter, $\alpha^2=\omega\rho_f 2/\mu_f$ is the viscosity parameter, $S=k/h^2$ is the Darcy parameter, and ϕ is the nanoparticles volume fraction.

By analytically solving Eq. (20) with the boundary conditions (21), we achieve:

$$f(\eta)=\left(\frac{\left(1+\sqrt{\Delta}(-1+y)cot\left[\sqrt{\Delta}\right]-cosec\left[\sqrt{\Delta}\right]sin\left[\sqrt{\Delta}y\right]\right)}{-2+2\sqrt{\Delta}cot\left[\sqrt{\Delta}\right]}\right)e^{iwt}, \tag{22}$$

where, $$\Delta=\left(2K_r\frac{A_1}{A_2}-\alpha^2h\frac{A_1}{A_2}-M^2\frac{A_3}{A_2}\left(\sin^2(\theta)\right)-\frac{1}{S}\right).$$

And

$$A_1=1-\phi+\phi\frac{\rho_s}{\rho_f},\ A_2=\frac{1}{(1-\phi)^{2.5}},\ A_3=1+\frac{3\left(\frac{\sigma_s}{\sigma_f}-1\right)\phi}{\left(\frac{\sigma_s}{\sigma_f}+2\right)-\left(\frac{\sigma_s}{\sigma_f}-1\right)\phi}.$$

Replacing $f(\eta)$ in the axial velocity u and radial velocity v becomes

$$u=\left[U(0)-\frac{xv_0}{h}\right]f'(\eta)\ and\ v=-v_0f(\eta)e^{iwt}. \tag{23}$$

The axial velocity components become

$$u(x,y)=\left[U(0)-\frac{xv_0}{h}\right]\left(\frac{\left(\sqrt{\Delta}\right)cosh\left(\sqrt{\Delta}y\right)-\left(\left(\sqrt{\Delta}\right)cosh\left(\sqrt{\Delta}\right)\right)}{2\left(sinh\left(\sqrt{\Delta}\right)-\left(\sqrt{\Delta}\right)cosh\left(\sqrt{\Delta}\right)\right)}\right)e^{iwt}. \tag{24}$$

The radial velocity components become

$$v(x,y)=\left[v_0e^{iwt}\right]\left(\frac{\left(1+\sqrt{\Delta}(-1+y)cot\left[\sqrt{\Delta}\right]-cosec\left[\sqrt{\Delta}\right]sin\left[\sqrt{\Delta}y\right]\right)}{-2+2\sqrt{\Delta}cot\left[\sqrt{\Delta}\right]}\right). \tag{25}$$

3. Pressure distribution

$$dp=\frac{\partial p}{\partial x}dx+\frac{1}{h}\frac{\partial p}{\partial\eta}d\eta, \tag{26}$$

$$\begin{aligned}dp=&\left[U(0)-\frac{xv_0}{h}\right]\left\{\left(\rho_{nf}2\Omega_{nf}-\rho_{nf}i\omega_{nf}-\rho_{nf}\frac{v_{nf}}{k}-B^2Sin^2\theta\sigma_{nf}\right)f'(\eta)-\frac{\rho_{nf}v_{nf}}{h^2}f'''(\eta)dx\right\}+\\&\left\{\frac{v_{nf}\rho_{nf}v_0f'(\eta)}{h^2}-\left(i\omega_{nf}v_0\rho_{nf}\right)f'(\eta)\right\}d\eta.\end{aligned} \tag{27}$$

Integrating the above equation

$$\begin{aligned}P(x,y)=&\left[hU-\frac{v_0x}{2h}\right]\left\{\left(\rho_{nf}2\Omega_{nf}-\rho_{nf}i\omega_{nf}-\rho_{nf}\frac{v_{nf}}{K}-B^2Sin^2\theta\sigma_{nf}\right)f'(\eta)+\frac{v_{nf}}{h^2}\rho_{nf}f'''(\eta)\right\}+\\&\left\{\frac{v_{nf}\rho_{nf}v_0}{h^2}f'(\eta)-\left(i\omega_{nf}v_0\rho_{nf}\right)f(\eta)\right\}d\eta\end{aligned} \tag{28}$$

4. Results and discussion

The analysis involves the movement of magnetized nanoliquid between parallel plates made of metallic silver. One of the plates is a smooth silver plate moving steadily, while the lower porous silver plate experiences uniform-speed suction. Figs. 2-14 are presented for this purpose. Furthermore, the results of the present study are in good agreement with the results available in the literature [21], which suggest the validity of the present model. The influence of dissimilar values ωt on the axial speed curve of the stream relation is demonstrated in Fig. 2. It is noted that the profile exhibits symmetry around the axes. Observing symmetry around the axes, we find that for an intermediate entry velocity of $U = 0.65$, along with consistent values of $\phi = 0.04$, $\alpha = 1$, $h = 1$, $M = 1$, $\theta = 1$, $s = 2$, $K_r = 3$, $v_0 = 0.7$, and $x = 3$, the axial velocity reductions from the upper plate towards the central of the plate. It shows an increase from the mid of the plate to the lower plate. At $\omega t = \pi/2$, the axial velocity displays a linear pattern, whereas for the other ωt values, it takes on a parabolic configuration. Fig. 3 depicts the change in radial velocity for the different values of ωt. Considering an average approach speed $U = 0.45$, along with consistent $\alpha = 1$, $h = 1$, $M = 1$, $\theta = 1$, $s = 2$, $K_r = 3$, $v_0 = 0.7$, and $x = 3$, the radial velocity diminishes from the upper plate to the lower plate. When $\omega t = 0$, the axial velocity becomes zero. Fig. 4 displays the variation in axial velocity for dissimilar values of the Rotation Parameter K_r. It shows that an upsurge in the Rotation Parameter K_r results in a reduction of axial velocity. Due to U being smaller than v_0, the Rotation Parameter acts to slow down the axial velocity profile. Fig. 5 illustrates the transverse velocity's variation corresponding to dissimilar values of the Rotation Parameter K_r. This pattern displays a two-fold symmetry. An escalation in K_r leads to an augmentation of line of sight velocity from the higher part of the plate to the inside part of the conduit, followed by a decrease from the middle section to the worse part of the plate. Notably, the x-axis velocity achieves its extreme in the higher part of the conduit and exhibits an opposing behavior in the lower half. In Fig. 6, the influence of α the axial velocity is depicted. As the α increases, the nanofluid axial velocity enhances. Fig. 7 presents the x-axis velocity corresponding to dissimilar values of parameter α. A distinct double-folded pattern characterizes this profile. With consistent parameters of $\alpha = 1$, $h = 1$, $M = 1$, $\theta = 1$, $s = 2$, $K_r = 3$, $v_0 = 0.7$, and $x = 3$, it's observed that as the value of α increases, the transverse velocity experiences a decline within the range $1 \le y \le 0$. Conversely, in the range $0 \le y \le -1$, an increase leads to an augmentation of the transverse velocity. Fig. 8 demonstrates the impact of rising values of M tends to an increase in axial velocity. Fig. 9 illustrates the two and three-dimensional radial velocity profile for different magnetic numbers causing the line of sight velocity to diminish from the higher part to the central of the conduit. However, from the center of the conduit to the worse part of the plate, the radial velocity experiences an increase. Fig. 10 illustrates the two and three dimensions impact of different values of ϕ tends to an decrease in axial velocity. Fig. 11 shows that the radial velocity profile declines with an upsurge of ϕ. Contours depicting dissimilar values of the concentration parameter ϕ and magnetic parameter M are shown in Figs. 12 to 13. Within the fluid's flow, a trend towards confinement within streamlines leads to a phenomenon referred to as trapping. The volume of trapped fluid is termed the bolus. Streamlines for $\phi = 0$ and $\phi = 0.04$ are displayed in Fig. 12(a-b). This analysis reveals that, in comparison to a Magnetic oxide, the number of bolus is larger in the case of water. Fig. 13(a-b) demonstrates that an upsurge in M results in a stretched trapped bolus while the circulation count increases.

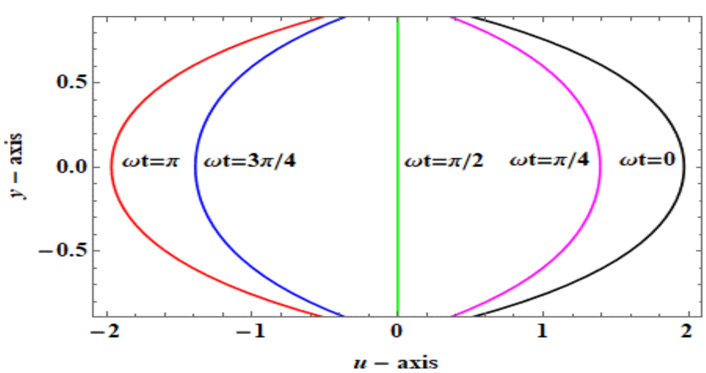

Fig. 2: Deviation of ωt on axial velocity with $\alpha = 1$, $h = 1$, $M = 1$, $\theta = 1$, $s = 2$, $K_r = 3$, $v_0 = 0.7$, $x = 3$, and $U = 0.7$.

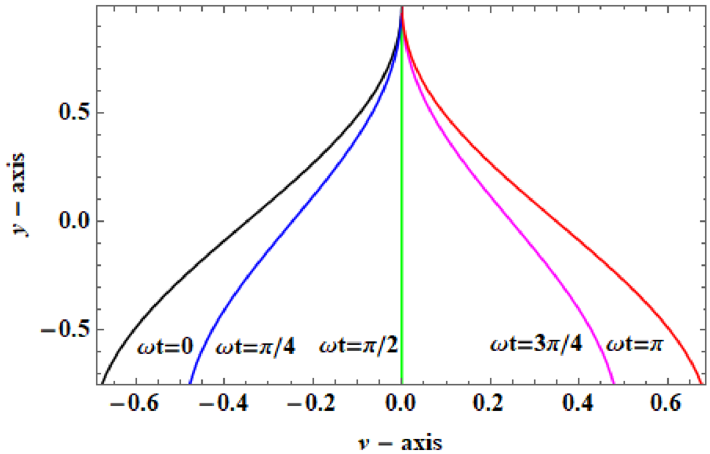

Fig. 3: Deviation of ωt on radial velocity with $\alpha = 1$, $h = 1$, $M = 1$, $\theta = 1$, $s = 2$, $K_r = 3$, $v_0 = 0.7$, $x = 3$, and $U = 0.7$.

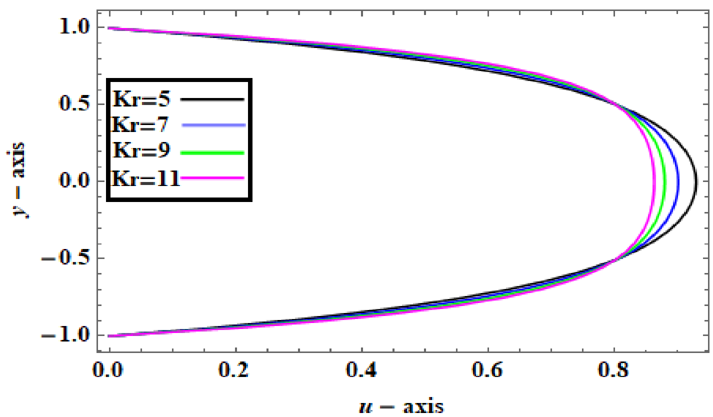

Fig. 4: Deviation of K_r on axial velocity with $\alpha = 1$, $h = 1$, $M = 1$, $\theta = 1$, $s = 2$, $K_r = 3$, $v_0 = 0.7$, $x = 3$, and $U = 0.7$.

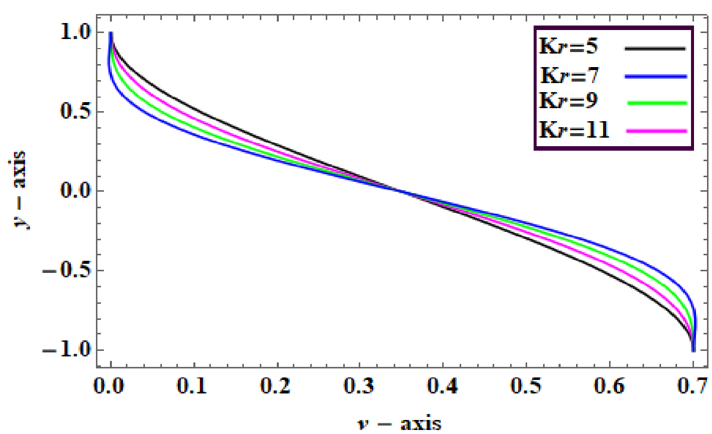

Fig. 5: Variation of K_r on radial velocity with $\alpha = 1$, $h = 1$, $M = 1$, $\theta = 1$, $s = 2$, $K_r = 3$, $v_0 = 0.7$, $x = 3$, and $U = 0.7$.

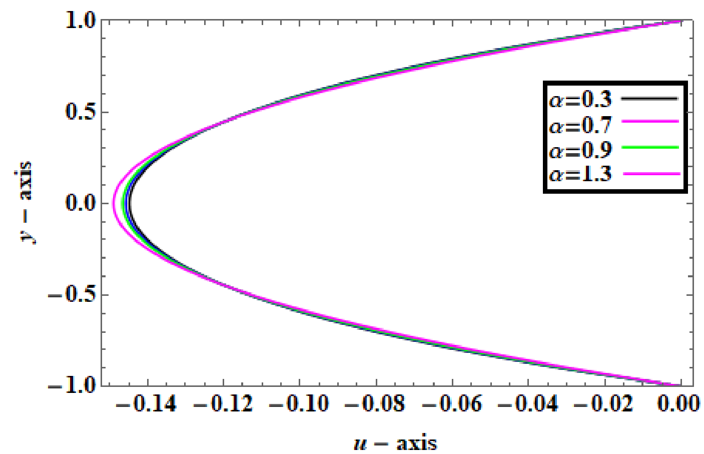

Fig. 6: Deviation of α on axial velocity with $\alpha=1$, $h=1$, $M=1$, $\theta=1$, $s=2$, $K_r=3$, $v_0=0.7$, $x=3$, and $U=0.7$.

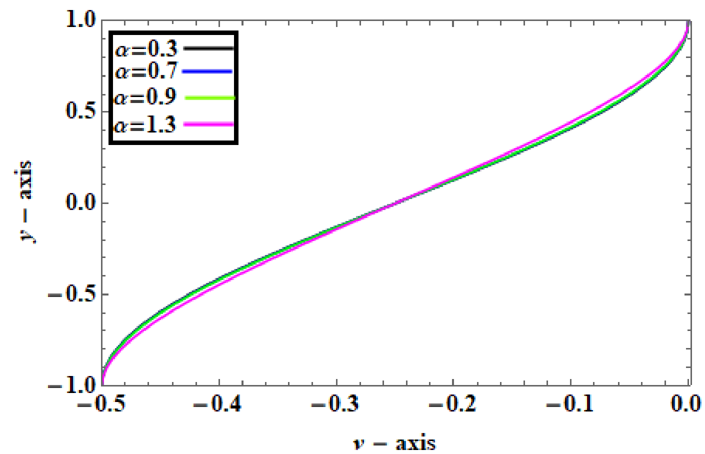

Fig. 7: Deviation of α on radial velocity with $\alpha=1$, $h=1$, $M=1$, $\theta=1$, $s=2$, $K_r=3$, $v_0=0.7$, $x=3$, and $U=0.7$.

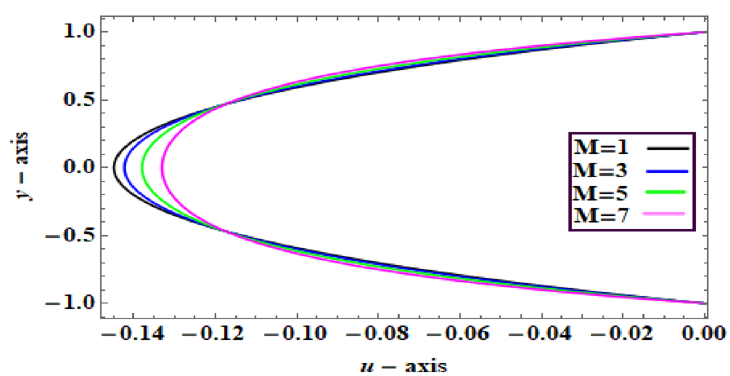

Fig. 8: Deviation of Magnetic Number M on axial velocity with $\alpha=1$, $h=1$, $M=1$, $\theta=1$, $s=2$, $K_r=3$, $v_0=0.7$, $x=3$, and $U=0.7$.

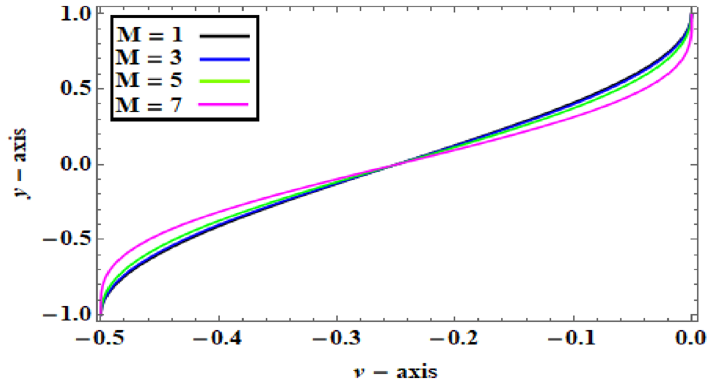

Fig. 9: Deviation of Magnetic Number M on radial velocity with $\alpha = 1$, $h = 1$, $M = 1$, $\theta = 1$, $s = 2$, $K_r = 3$, $v_0 = 0.7$, $x = 3$, and $U = 0.7$.

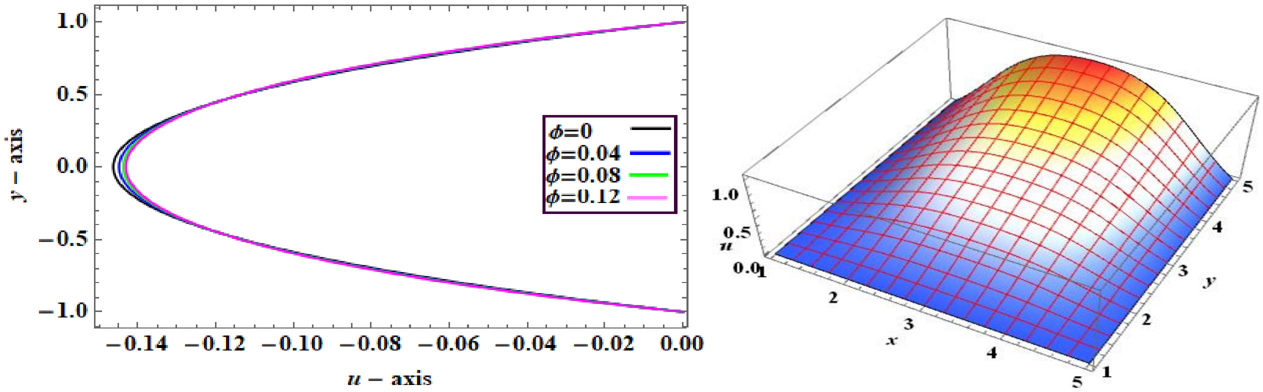

Fig. 10: Deviation of ϕ on axial velocity with $\alpha = 1$, $h = 1$, $M = 1$, $\theta = 1$, $s = 2$, $K_r = 3$, $v_0 = 0.7$, $x = 3$, and $U = 0.7$.

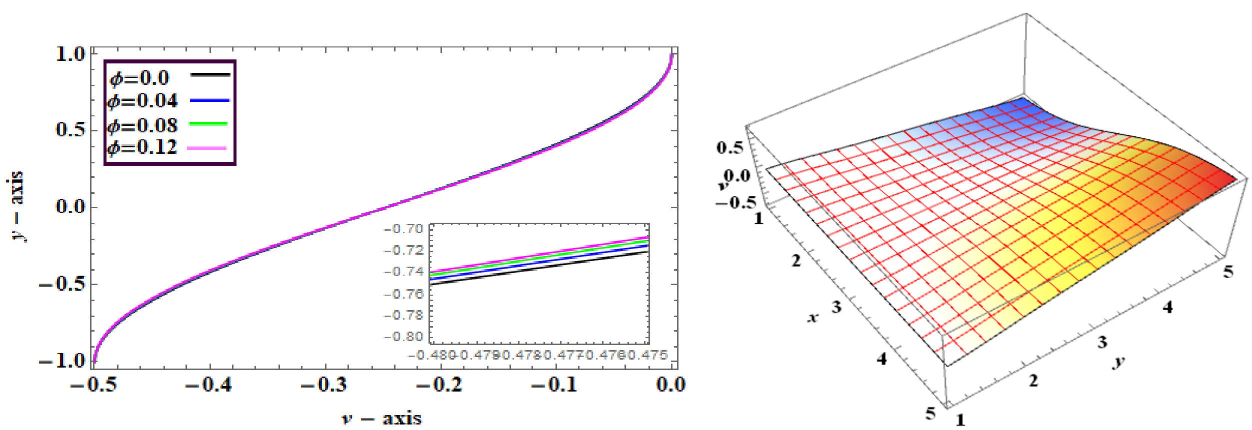

Fig. 11: Deviation of ϕ on radial velocity with $\alpha = 1$, $h = 1$, $M = 1$, $\theta = 1$, $s = 2$, $K_r = 3$, $v_0 = 0.7$, $x = 3$, and $U = 0.7$.

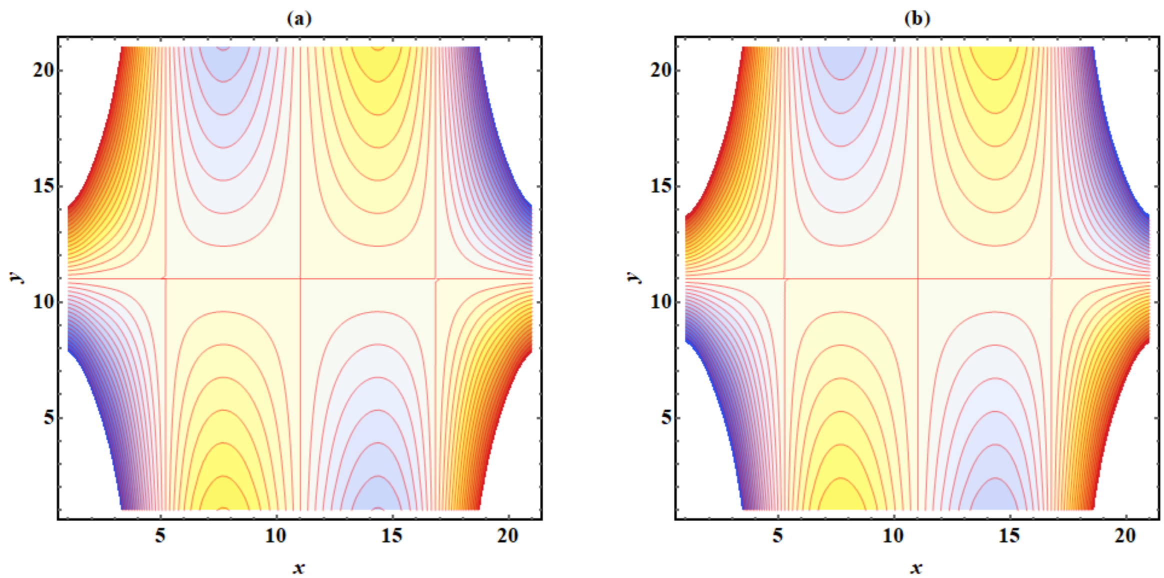

Fig. 12: Contours of the water (a) $\phi = 0.0$ and Magnetic oxide (b) $\phi = 0.04$.

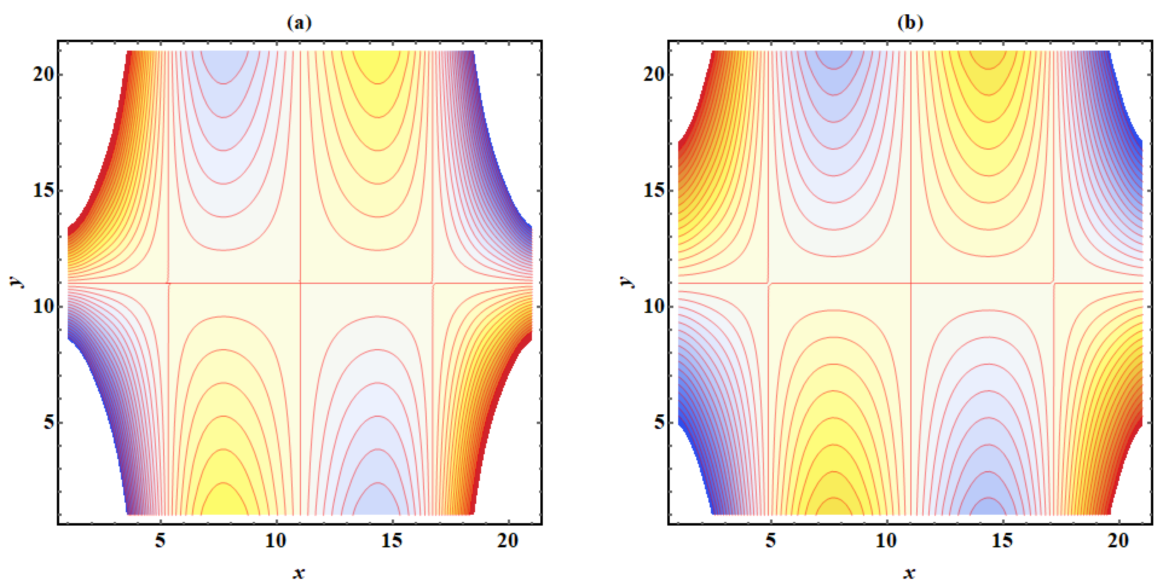

Fig. 13: Contours for (a) $M = 0.5$ and (b) $M = 1.5$.

5. Validation

This segment aims to validate the exactness of our results. To confirm the attained outcomes, we compare the limiting case of the current inquiry, specifically the axial and radial velocity profile in the absence of nanoparticles volume fraction, with the outcomes presented by Anand et al. [21] (refer to Figure 14). The graph illustrates that there is a satisfactory agreement between both sets of findings.

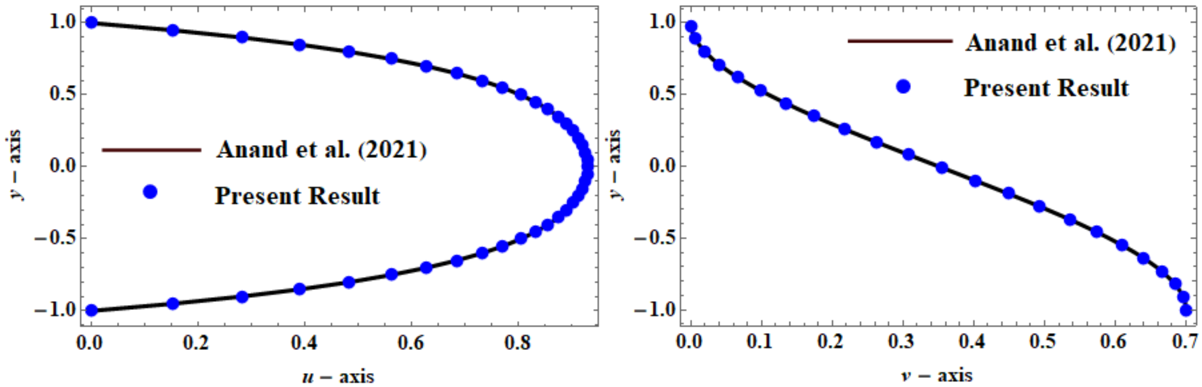

Fig. 14: Contrasting the extreme scenario of our current investigation with the outcomes from [21].

6. Conclusions

The influence of hydromagnetic viscous nanofluid transport between parallel silver plates in which constant periodic suction takes place at the lower plate and the upper plate is moving uniformly. This hypothetical application model illustrates the potential of incorporating magnetic oxide nanoparticles into a Couette flow system to pioneer inventive solutions in domains like control of fluid dynamics, and intelligent lubrication across diverse engineering and industrial applications. The flow field equations have transformed to non-dimensional from exhausting appropriate similarity variables. A closed-form solution is attained for the axial velocity and radial velocity. During the transformation of the modeled system, several physical parameters have been incorporated. The impacts of these parameters are visually presented through figures and comprehensively discussed. The primary outcomes of the existing inquiry are outlined as surveys:

- Elevating the Hartmann values leads to a rise in axial velocity across the entire flow region.
- Augmenting the Hartmann values leads to a reduction in radial velocity from the upper plate to the middle portion, followed by an increase from the center of the conduit towards the lower porous plate.The application of a transverse magnetite field, oriented orthogonally to the flow direction, induces a resistive force referred to as the Lorentz force. This force acts in opposition to the nanofluid flow, leading to a reduction in velocity. The Lorentz force exhibits a propensity to decelerate the fluid motion within the boundary layer. These findings align quantitatively with anticipated outcomes, as the magnetic field imposes a retarding force on the natural convection flow.
- Raising the suction parameter results in a parabolic increase in axial velocity.
- With an upsurge in the suction parameter, the radial velocity experiences a decline in the upper region of the plates and a subsequent rise in the lower parallel portion of the plates.
- The axial velocity reduces with augmenting values of the rotation parameter. However, the transverse velocity rises where $y \in [0,1]$ and diminutions where $y \in [-1,0]$.
- Altering the volume fraction of nanoparticles results in a decrease in the axial velocity profile and a simultaneous reduction in the radial velocity. The utilization of nanofluids is being investigated for its capacity to improve the efficiency of energy systems. Researchers seek to optimize fluid flow in systems such as solar collectors or nuclear reactors by customizing the axial velocity profile in nanofluids.
- In future works, the utilization of a hybrid nanofluid model can be explored for addressing heat transfer phenomena and solving associated heat transfer problems.

References

[1] S. U. S. Choi, D. A. Singer, and H. P. Wang, “Developments and applications of non-Newtonian flows,” *ASME Fluids Engineering Division*, vol. 66, pp. 99–105, 1995.

[2] M. Sheikholeslami and D. D. Ganji, “Heat transfer of Cu-water nanofluid flow between parallel plates,” *Powder Technology*, vol. 235, pp. 873–879, 2013.

[3] R. Ahmad, M. Mustafa, and M. Turkyilmazoglu, “Buoyancy effects on nanofluid flow past a convectively heated vertical Riga-plate: A numerical study,” *International Journal of Heat and Mass Transfer*, vol. 111, pp. 827–835, 2017.

[4] S. E. Awan, M. A. Z. Raja, F. Gul, Z. A. Khan, A. Mehmood, and M. Shoaib, "Numerical computing paradigm for investigation of micropolar nanofluid flow between parallel plates system with impact of electrical MHD and Hall current," *Arabian Journal for Science and Engineering*, vol. 46, pp. 645–662, 2021.

[5] S. Sivasankaran, T. Chandrapushpam, M. Bhuvaneswari, S. Karthikeyan, and A. K. Alzahrani, "Effect of chemical reaction on double diffusive MHD squeezing copper water nanofluid flow between parallel plates," *Journal of Molecular Liquids*, vol. 368, pp. 120768, 2022.

[6] M. Nazeer, K. Ramesh, H. Farooq, and Q. Shahzad, "Impact of gold and silver nanoparticles in highly viscous flows with different body forces," *International Journal of Modelling and Simulation*, vol. 43, pp. 376–392, 2023.

[7] R. A. Talarposhti, Z. Asadi, H. Rezazadeh, D. D. Ganji, and A. Bekir, "Analytical solution for differential nonlinear and coupled equations in micropolar nanofluid flow between rotating parallel plates," *European Physical Journal Special Topics*, vol. 228, pp. 2601–2617, 2019.

[8] Z. Abbas, T. Mushtaq, S. A. Shehzad, A. Rauf, and R. Kumar, "Slip flow of hydromagnetic micropolar nanofluid between two disks with characterization of porous medium," *Journal of the Brazilian Society of Mechanical Sciences and Engineering*, vol. 41, 2019.

[9] Z. Abbas, S. Hussain, M. Y. Rafiq, and J. Hasnain, "Oscillatory slip flow of Fe3O4 and Al2O3 nanoparticles in a vertical porous channel using Darcy's law with thermal radiation," *Heat Transfer Research*, vol. 49, pp. 3228–3245, 2020.

[10] S. Gajbhiye, A. Warke, and K. Ramesh, "Mathematical modeling and analysis of immiscible metallic-based nanofluid flow in a microchannel with non-spherical nanoparticles," *Mathematics and Computers in Simulation*, vol. 213, pp. 40-54, 2023.

[11] G. Palani and I. A. Abbas, "Free convection MHD flow with thermal radiation from an impulsively-started vertical plate," *Nonlinear Analysis: Modelling and Control*, vol. 14, pp. 73–84, 2009.

[12] A. Tassaddiq, "MHD flow of a fractional second grade fluid over an inclined heated plate," *Chaos, Solitons & Fractals*, vol. 123, pp. 341–346, 2019.

[13] Z. Abbas, J. Hasnain, and M. Sajid, "Effects of slip on MHD flow of a dusty fluid over a stretching sheet through porous space," *Journal of Engineering Thermophysics*, vol. 28, pp. 84–102, 2019.

[14] Z. Shoukat, M. H. Zubair, M. Farman, A. Akgül, M. Sultan, S. S. Sharipov, and H. Algarni, "Impacts of joule heating with Cattaeno-Christove heat flux model in a MHD flow of Erying-Powell fluid on a Riga plate," *Alexandria Engineering Journal*, vol. 64, pp. 741–748, 2023.

[15] A. S. Rashed, S. M. Mabrouk, and A. M. Wazwaz, "Unsteady three-dimensional laminar flow over a submerged plate in electrically conducting fluid with applied magnetic field," *Waves in Random and Complex Media*, vol. 33, pp. 505–524, 2023.

[16] Z. I. Butt, I. Ahmad, M. Shoaib, H. Ilyas, and M. A. Z. Raja, "A novel design of inverse multiquadric radial basis neural networks to analyze MHD nanofluid boundary layer flow past a wedge embedded in a porous medium under the influence of radiation and viscous effects," *International Communications in Heat and Mass Transfer*, vol. 140, pp. 106516, 2023.

[17] T. Hayat, T. Muhammad, A. Alsaedi, and M. S. Alhuthali, "Magnetohydrodynamic three-dimensional flow of viscoelastic nanofluid in the presence of nonlinear thermal radiation," *Journal of Magnetism and Magnetic Materials*, vol. 385, pp. 222–229, 2015.

[18] M. Sheikholeslami, T. Hayat, T. Muhammad, and A. Alsaedi, "RETRACTED: MHD forced convection flow of nanofluid in a porous cavity with hot elliptic obstacle by means of Lattice Boltzmann method," vol. 135, pp. 532-540, 2018.

[19] H. R. Patel, "Effects of heat generation, thermal radiation, and hall current on MHD Casson fluid flow past an oscillating plate in porous medium," *Multiphase Science and Technology*, vol. 31, no. 1, pp. 87-107, 2019.

[20] Z. Abbas, M. Naveed, M. Hussain, and N. Salamat, "Analysis of entropy generation for MHD flow of viscous fluid embedded in a vertical porous channel with thermal radiation," *Alexandria Engineering Journal*, vol. 59, pp. 3395–3405, 2020.

[21] V. W. J. Anand, S. Ganesh, P. Chandrasekar, J. Jayaraman, and A. Mariadhas, "Unsteady MHD Couette viscous fluid flow through silver metallic parallel plates with an inclined magnetic field and angular velocity subjected to constant suction at lower plate," *Materials Today: Proceedings*, vol. 44, pp. 3919–3923, 2021.

[22] B. Jalili, S. Sadighi, P. Jalili, and D. D. Ganji, "Numerical analysis of MHD nanofluid flow and heat transfer in a circular porous medium containing a Cassini oval under the influence of the Lorentz and buoyancy forces," *Heat Transfer Research*, vol. 51, pp. 6122–6138, 2022.

[23] S. Abbas, M. Nazar, Z. U. Nisa, M. Amjad, S. M. E. Din, and A. M. Alanzi, "Heat and mass transfer analysis of MHD Jeffrey fluid over a vertical plate with CPC Fractional derivative," *Symmetry*, vol. 14,pp. 2491, 2022.

[24] Z. Abbas, A. U. Rehman, S. Khaliq, and M. Y. Rafiq, "Flow dynamics of MHD hybrid nanofluid past a moving thin needle with a temporal stability test: A Galerkin method approach," *Numerical Heat Transfer, Part B: Fundamentals*, pp. 1–19, 2023.

[25] M. S. Arslan, Z. Abbas, M. Y. Rafiq, and J. Hasnain, "Metachronal wave analysis for magnetized Williamson fluid through a ciliated curved channel," *Proceedings of the Institution of Mechanical Engineers, Part E: Journal of Process Mechanical Engineering*, 2024.

[26] B. Ali, S. Jubair, Z. Mahmood, N. A. Koka, and A. H. Gani, "Analysis of unsteady MHD fluid flow across two parallel discs with uniform fluctuation subject to modified Hall and activation energy," *International Journal of Modern Physics B*, vol. 38, no. 31, pp. 2450424, 2024.

[27] Z. M. Mburu, S. A. Ogutu, S. Mondal, and P. Sibanda, "Entropy production in unsteady MHD double diffusive and chemically reactive nanofluid flow past a rotating permeable plate using overlapping grid spectral collocation technique," *International Journal of Ambient Energy*, vol. 45, pp. 2280743, 2024.